

## Electronic Supplementary Information

### Band Gap and Photo Charge Carrier Tailoring in Zr-Doped Carbon Nitride Using ZrCl<sub>4</sub>-DMF-Melamine for Photocatalytic Degradation of Rhodamine B

*Chinathun Pinming<sup>a,†</sup>, Qingshan Yang<sup>a,†</sup>, Navaphun Kayunkid<sup>b</sup>, Visittapong Yordsri<sup>c</sup>, Winadda  
Wongwiriyan<sup>b,\*</sup>, Young Jae Song<sup>a,d,e,f,\*</sup>*

<sup>a</sup>SKKU Advanced Institute of Nanotechnology (SAINT), Sungkyunkwan University (SKKU),  
Suwon Gyeonggi-do 16419, Republic of Korea

<sup>b</sup>College of Materials Innovation and Technology, King Mongkut's Institute of Technology  
Ladkrabang, Chalongkrung Rd., Ladkrabang, Bangkok, 10520, Thailand

<sup>c</sup>National Metal and Materials Technology Center (MTEC), 114 Thailand Science Park, Klong  
Luang, Pathum Thani 12120, Thailand

<sup>d</sup>Department of Nano Science and Technology, Sungkyunkwan University, Suwon16419,  
Republic of Korea

<sup>e</sup>Department of Nano Engineering, Sungkyunkwan University, Suwon16419, Republic of Korea

<sup>f</sup>Center for 2D Quantum Heterostructures, Institute for Basic Science (IBS), Suwon 16419,  
Republic of Korea

\*Corresponding author E-mail: winadda.wong@kmitl.ac.th, yjsong@skku.edu

## Experimental detail

### Materials and Chemicals

All materials and chemicals were of analytical grade and used without further purification. Melamine (99% Sigma Aldrich), zirconium tetrachloride ( $ZrCl_4$ , 98% Thermo Scientific chemicals), dimethylformamide (DMF, 99% Thermo Scientific Chemicals), fluorine-doped tin oxide substrate (FTO, Sigma Aldrich with surface resistivity of 6-7  $\Omega$ /square), Nafion solution (D-520, 5%w/w in water and propanol, Thermo Scientific Chemicals), rhodamine B (RhB, dye content 97%, Sigma Aldrich), and deionized water (DI)

### Synthesis of Zr doped carbon nitride

First, 2.5 g of melamine powder was dissolved in DMF solvent under heating at 100 °C and stirring rate of 500 rpm until the powder completely dispersed; next,  $ZrCl_4$  powder (1-3 mmol) as a Zr precursor was slowly added into the solution. The mixture was maintained under these conditions for 48 h to induce the cleavage of the  $ZrCl_4$  polymeric structure into a smaller structure and to form a complex molecular structure of the precursor. The unreacted and excess DMF solvent was washed out by washing with acetone and the precursor was separated by centrifugation at 4000 rpm for 5 minutes, repeating the process washing and separating for 3 times. Then, the precursor dried in a vacuum desiccator overnight. The dried precursor was placed in a semi-closed alumina crucible to synthesize the Zr-doped CN. The crucible was annealed at 600 °C for 4 h at a ramping rate of 5 °C/min under an argon flow of 100 sccm in the tubular furnace; the furnace was then allowed to cool down to room temperature naturally. To enhance the properties of the Zr-doped CN, as-prepared Zr-doped CN powder was heated in an air muffle furnace at 500 °C for 2 h at a ramping rate of 5 °C/min to exfoliate the CN structure and decompose the carbon impurities. Zr-doped CN with different amounts of Zr was referred to as  $Zr_x$ -CN (where x is the initial mmol of the  $ZrCl_4$  precursor). The C=O group in the DMF molecule is believed to form a bond with the oxophilic Zr atom. After

the thermal polycondensation process, the DMF molecules decompose under heat. It is proposed that some atoms from the DMF molecule can act as C and N sources, facilitating the incorporation of Zr into the carbon nitride structure formed during the thermal polycondensation of melamine.

### **Material characterization**

The morphology and crystallinity of the as-synthesized Zr-doped CN powder samples were observed using scanning electron microscopy with energy dispersive spectroscopy (SEM-EDX, JEOL, JSM-7800F) for elemental analysis, and the internal morphology and selected area electron diffraction (SAED) were observed using transmission electron microscopy (TEM, JEOL, JEM-3100F). The chemical composition and bonding information of the Zr-doped CN powder were determined using X-ray photoelectron spectroscopy (XPS) on a model of ESCALAB 250Xi-X-ray, using monochromated Al K $\alpha$  radiation as the exciting source. The as-synthesized Zr-doped CN powder was added to the pellet before the X-ray diffraction (XRD) and diffuse reflectance spectroscopy (DRS) measurements to facilitate characterization. The crystallinity of the Zr-doped CN was characterized by XRD analysis using a RIGAKU diffractometer in a theta/2theta with Cu K $\alpha$  ( $\lambda = 0.154$  nm) radiation. The bonding chemical information of the Zr-doped CN was obtained using an attenuated total reflectance Fourier transform infrared (ATR-FTIR) spectrophotometer (Shimadzu, IR Tracer-100) in the 600–4000 cm<sup>-1</sup> range. Optical band gap analysis was conducted in the DRS mode on a ultraviolet-visible (UV-Vis) spectrophotometer (Shimadzu, Solidspec-3700i DUV spectrophotometer) using barium sulfate (BaSO<sub>4</sub>) as the standard reference material. The time-resolved photoluminescence (TRPL) and steady photoluminescence spectra of the Zr-doped CN were obtained using a picosecond pulsed diode laser (BDL-375, Becker & Hickl GmbH) with a

wavelength of 375 nm and equipped with a 50 cm long monochromator equipped with a cooled-charge coupled device (CCD) (PIXIS 400, Princeton Instruments) and a time-correlated single-photon counting (TCSPS, Becker & Hickl GmbH) correlator. The specific surface area and porosity of the powdered Zr-doped CN were characterized by N<sub>2</sub> adsorption-desorption isotherms using the Barrett Joyner Halenda (BJH) and Brunauer Emmett Teller (BET) methods on a surface area and pore size analyzer (Quantachrome, Autosorb iQ-C-XR).

### **Photoelectrochemical (PEC) properties of the Zr-doped CN**

Photoelectrochemical (PEC) measurements, including a linear I-V scan, electrochemical impedance spectroscopy (EIS), transient photocurrent response (I-t), and Mott Schottky analysis, were performed in a glass cell equipped with a three-electrode system consisting of Zr-doped CN-coated FTO glass substrate as the working electrode, a saturated calomel electrode (SCE) as the reference electrode, and a Pt wire as the counter electrode. The electrolytic aqueous solution used for the PEC measurements was 1 mol of sodium sulfate (Na<sub>2</sub>SO<sub>4</sub>). All the PEC measurements were performed on an electrochemical workstation (Bio-logic VSP) controlled using EC-Lab v11.33 software. The light reaction of photoelectrochemical measurements was performed with a 300 W Xenon arc lamp with a UV filter ( $\lambda > 420$  nm) as an irradiation light source placed at a 20 cm distance from the PEC cell. The linear I-V scan was conducted between -0.2 and 1.1 V at a 5 mV scan rate in both light and dark conditions. The transient photocurrent response was performed at a constant potential of 0.8 V under controlled light irradiation, which was chopped manually. The electrochemical impedance spectrums were analyzed at a frequency of 1 MHz to 0.1 Hz at a fixed potential of 0.8 V in both light and dark conditions. Mott Schottky analysis was

performed at a fixed frequency of 1000 Hz under light illumination conditions. For working electrode fabrication, the working electrode was fabricated by drop-casting a slurry of the photocatalyst on an FTO substrate. A slurry of photocatalysts was prepared by suspending 7.5 mg of the photocatalyst dispersed in 1 mL ethanol and 50  $\mu$ L of 5 wt.% Nafion binder solution, followed by sonication for 60 min. After that, 200  $\mu$ L of the slurry was dropped onto the 1 $\times$ 1.5 cm<sup>2</sup> conductive surface of FTO, followed by annealing at 100  $^{\circ}$ C for 24 h to increase the adhesion and film quality

### **Photocatalytic efficiency of the Zr-doped CN**

The photocatalytic efficiency of the Zr-doped CN was investigated by the degradation of a RhB solution under irradiation by a commercial white-light LED with a power of 5 mW/cm<sup>2</sup> and a duty cycle of 30%. All experiments were performed in a 200 mL beaker with a working volume of 100 mL. In a typical experiment, the photocatalyst the Zr-doped CN (50 mg) was suspended in 100 mL of a 10 ppm RhB solution dissolved in DI water under stirring at 200 rpm at room temperature. Before light irradiation, the aqueous suspension was kept in the dark for 120 min to ensure that the photocatalyst reached the adsorption-desorption equilibrium of RhB on the surface. At the interval of irradiated time, 2 mL of the suspension was collected and filtered through a 0.45  $\mu$ m PTFE membrane before analyzing the RhB concentration using a ultraviolet-visible spectrophotometer in absorbance mode. For stability and recycling photocatalytic reactions, the optimized photocatalyst was collected and then irradiated with white light LEDs for 5 h to remove the residual RhB on the surface and dried at 100  $^{\circ}$ C before the next cycle of photocatalytic reaction. A scavenger testing experiment was conducted to investigate the reactive radical

species responsible for RhB degradation. The photodegradation of the RhB experiment was performed individually via the same process with further addition of 0.5 mM of scavengers, including benzoquinone (BQ), isopropanol (IPA), dimethyl sulfoxide (DMSO) and ethylene diamine tetraacetic acid (EDTA), as the superoxide radical ( $\bullet\text{O}_2^-$ ), hydroxyl radical ( $\bullet\text{OH}$ ), electron ( $e^-$ ) and hole ( $h^+$ ) scavengers, respectively.

(a)



(b)

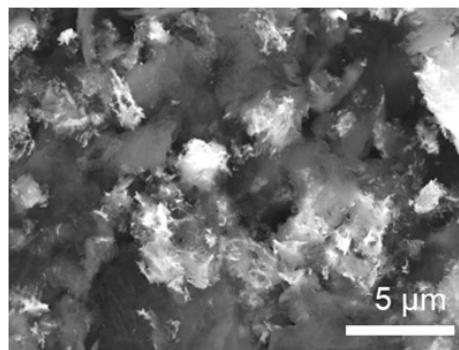


**Figure S1.** (a) Photograph of 25 mg amounts and (b) SEM micrographs of Zr<sub>1</sub>-CN, respectively.

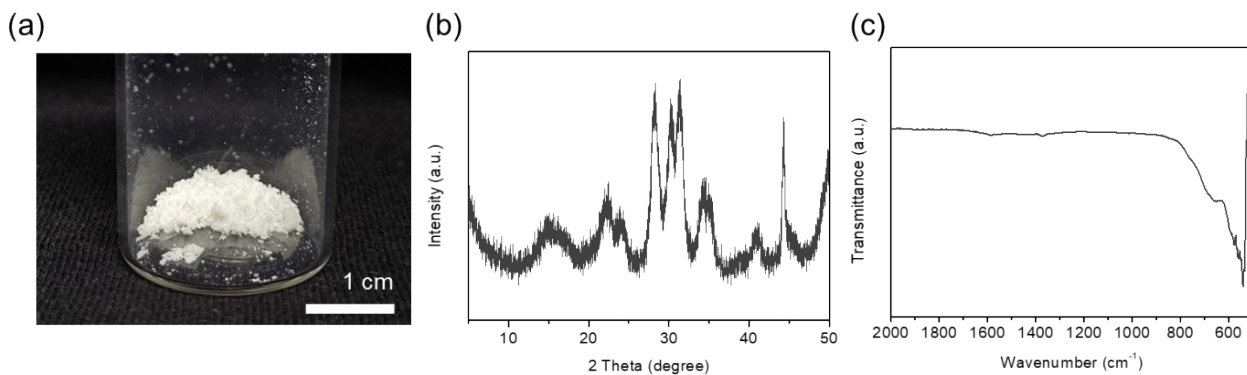


**Figure S2.** (a) Photograph of 25 mg amounts, (b) XRD pattern, and (c) FTIR spectra of synthesized powder obtained using 4 mmol  $ZrCl_4$  with DMF and melamine precursor.

Figure S2 shows the XRD pattern of amorphous carbon,  $ZrO_2$ , with various crystal orientations and no characteristic peaks of CN. The FTIR spectra also show no characteristic peak of CN in the  $1000\text{--}1700\text{ cm}^{-1}$  wavelength range, indicating that the CN structure might have disintegrated by the dissociation of the Cl atom while the precursor was heating in the furnace.

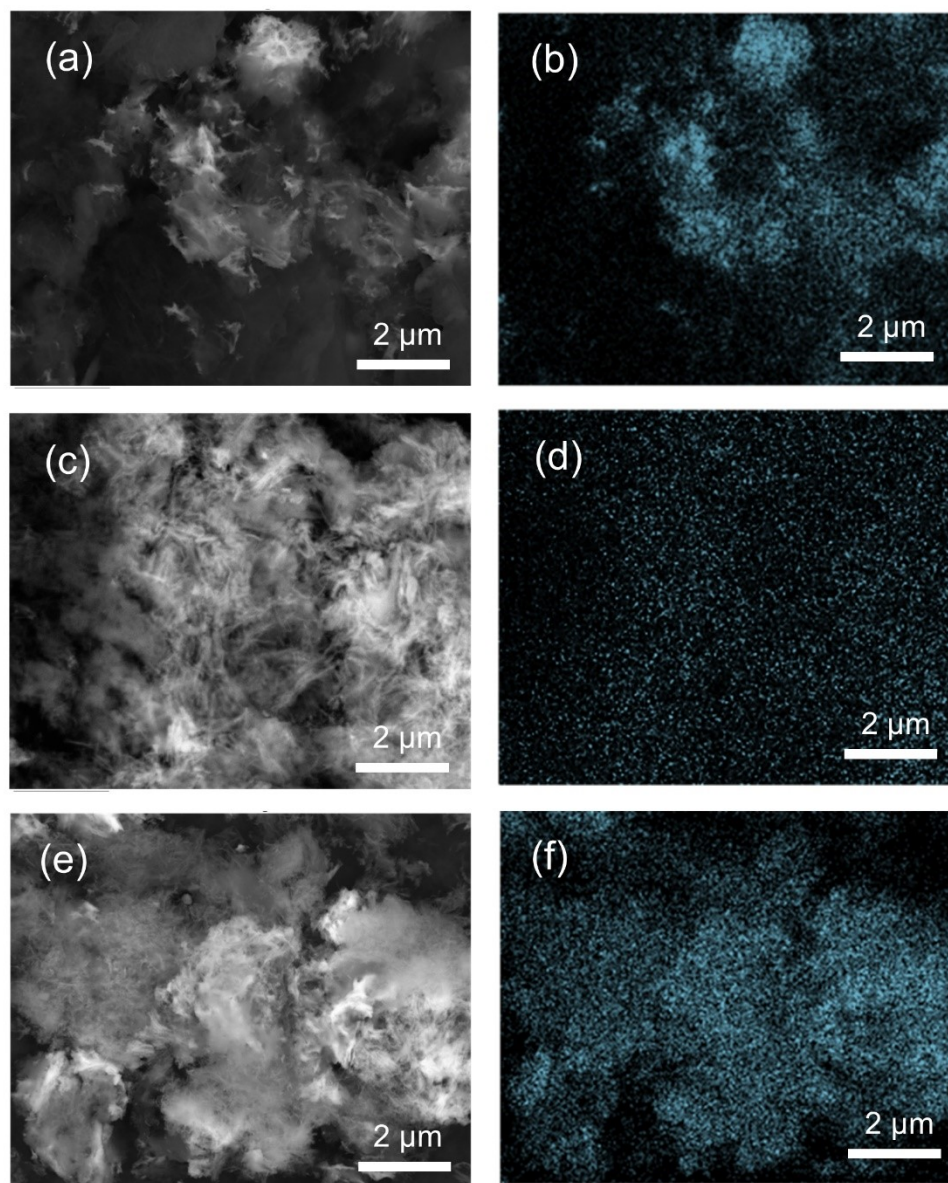


**Figure S3.** The SEM micrographs and EDS mapping analysis of the Zr atom of (a,b) Zr<sub>1</sub>-CN, (c,d) Zr<sub>2</sub>-CN, and (e,f) Zr<sub>3</sub>-CN, respectively.

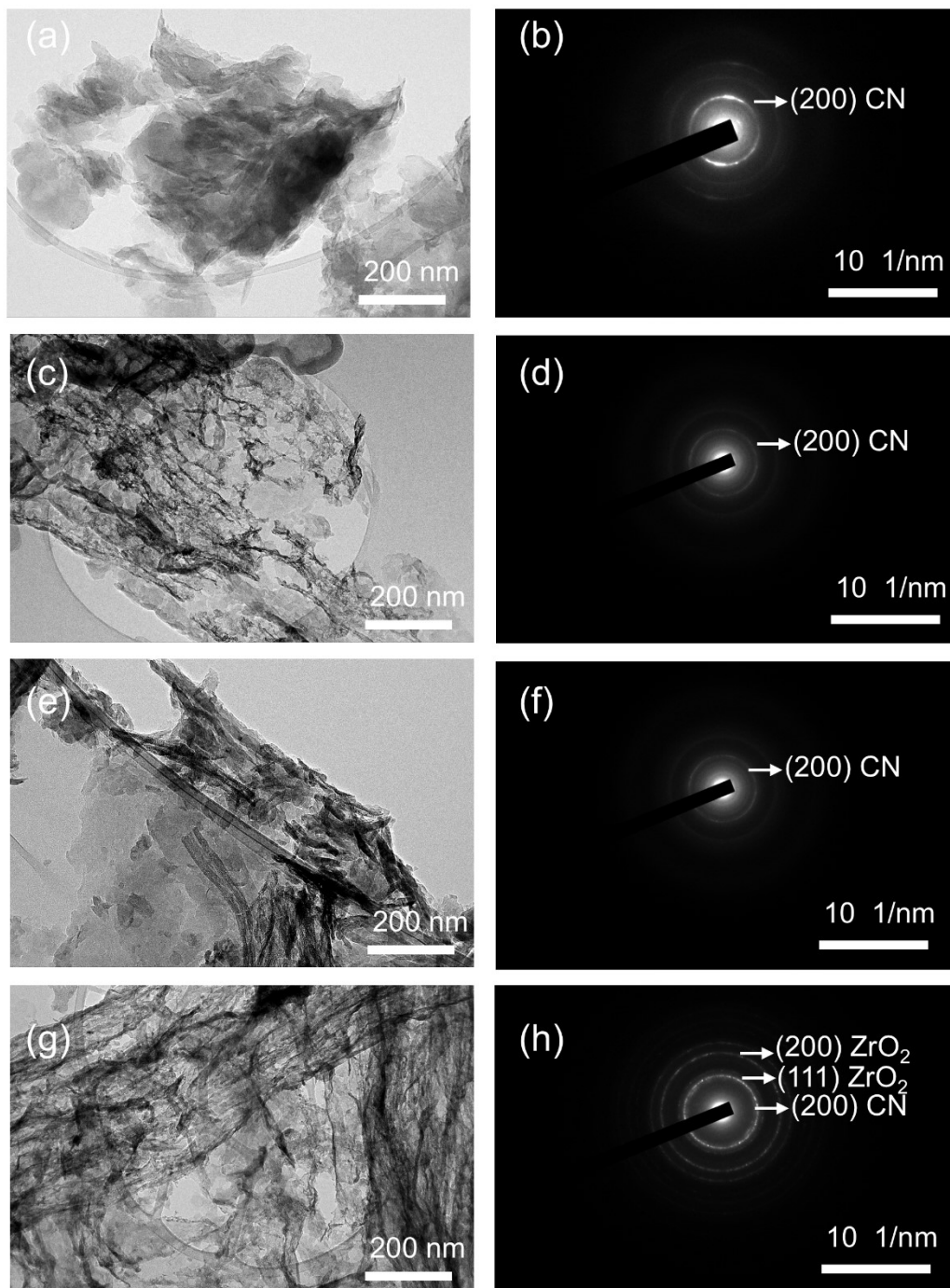


**Figure S4.** The TEM micrographs and SAED analysis of (a,b) CN, (c,d)  $Zr_1$ -CN, (e,f)  $Zr_2$ -CN, and (g,h)  $Zr_3$ -CN, respectively.

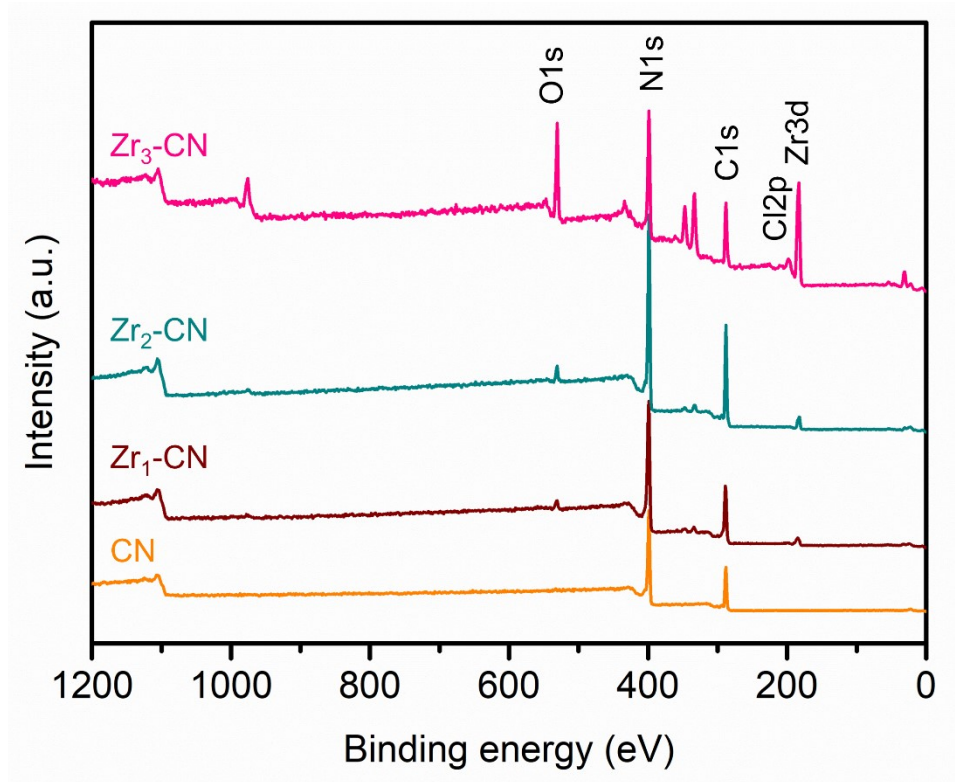


**Figure S5.** The survey scan of XPS spectra of all elements of the Zr-doped CN.

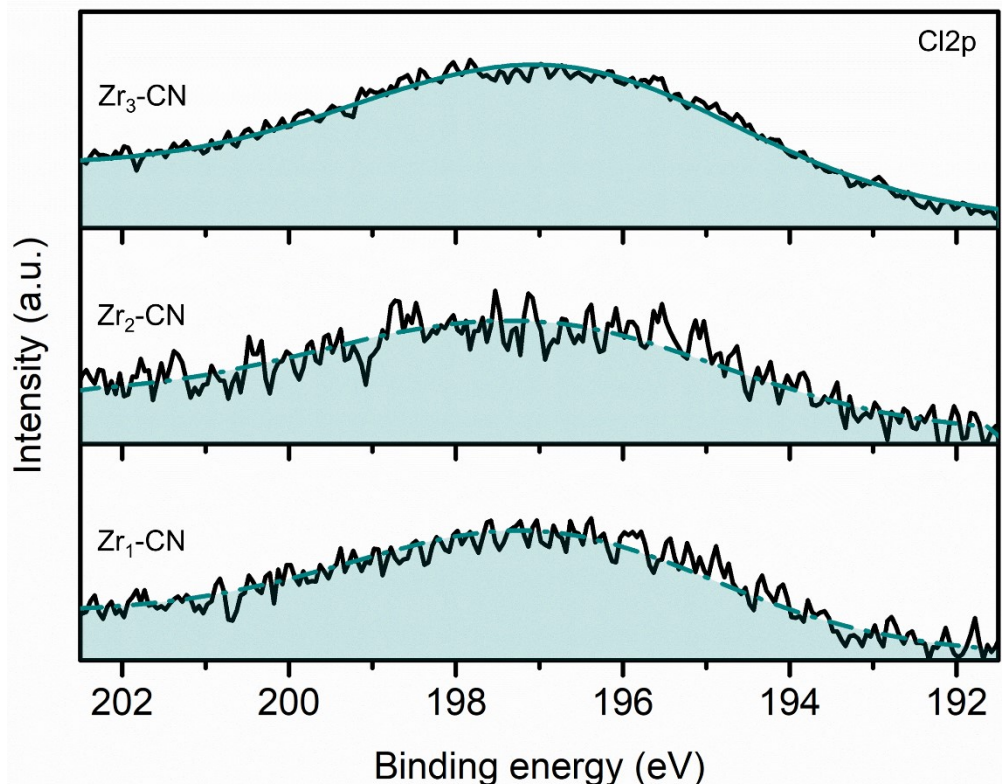


**Figure S6.** High-resolution XPS spectra of Cl2p of the Zr-doped CN photocatalyst.

For the Cl2p XPS peak (Figure S6), a single peak was observed at 197 eV, attributed to the ionic chloride ion species.<sup>1-3</sup> Based on the XPS results, the chloride ions do not form covalent bonds with carbon or nitrogen atoms, as indicated by the absence of a peak at 199 eV, which corresponds to the C-Cl bond,<sup>1,2</sup> suggesting that chloride ions exist in the form of negatively charged ions ( $\text{Cl}^-$ ) and may exhibit ionic interactions with  $\text{Zr}^{4+}$  ions or act as interstitial ions within the layers of CN.

**Table S1.** The atomic percentage and C/N ratio of the Zr-doped CN photocatalyst.

Samples	%C	%N	%Zr	%O	%Cl	C/N ratio
CN	41.05	57.71	-	1.09	-	0.71
Zr <sub>1</sub> -CN	39.86	55.76	0.84	3	0.5	0.71
Zr <sub>2</sub> -CN	40.12	55.43	1.29	2.49	0.7	0.72
Zr <sub>3</sub> -CN	31.58	37.75	7.21	19.4	4.1	0.84

**Table S2.** The deconvoluted XPS BE peak of C1s, Cl2p, O1s, and the ratio of Zr-O to O surface of the Zr-doped CN photocatalyst.

Samples	C1s			Cl2p	O1s		
	N-C=N (FWHM)	C-O/C=O (FWHM)	C-C bond (FWHM)	Ionic Cl (FWHM)	O-H surface (FWHM)	Zr-O (FWHM)	Zr-O peak to O surface ratio
CN	288 (1.03)	-	-	-	532.2 (2.6)	-	-
Zr <sub>1</sub> -CN	288.1 (1)	-	285 (1.08)	199.9 (5.13)	531.8 (2.17)	530.4 (1.68)	0.48
Zr <sub>2</sub> -CN	288.15 (0.97)	-	284.7 (0.89)	199.7 (5.62)	532.17 (2.49)	530.35 (1.7)	0.89
Zr <sub>3</sub> -CN	287.83 (1.07)	285.8 (2.8)	284.6 (1.12)	196.7 (5.33)	531.8 (2.46)	530.2 (1.82)	1.74

**Table S3.** The deconvoluted XPS peak of N1s and ratio of N species of the Zr-doped CN photocatalyst.

Samples	Pyridinic	Graphitic	Pyrrolic	$\pi$ excitation	Ratio of Pyridinic to Graphitic	Ratio of Pyridinic to Pyrrolic
	Peak BE (FWHM)	Peak BE (FWHM)	Peak BE (FWHM)	Peak BE (FWHM)		
CN	398.5 (1.05)	399.9 (1.8)	401.1 (0.98)	404.1 (2.46)	2.99	8.2
Zr <sub>1</sub> -CN	398.65 (1.02)	400 (2.08)	401.3 (0.89)	404.1 (1.71)	2.42	8.3
Zr <sub>2</sub> -CN	398.6 (1.01)	399.9 (1.81)	401.2 (0.94)	404.1 (2.6)	2.34	10.86
Zr <sub>3</sub> -CN	398.35 (1.13)	399.6 (2.62)	400.9 (0.92)	403.5 (1.61)	2.19	19.47

Upon examining the ratios of the integrated peak areas of pyridinic to graphitic nitrogen and pyridinic to pyrrolic nitrogen, increasing the Zr doping concentration decreased the pyridinic to graphitic ratio from 2.99 to 2.19, as explained by the high chemical activity of pyridinic nitrogen, which possesses a lone pair of electrons in its p orbitals that can interact with the Zr-ion dopants. This interaction reduced the proportion of pyridinic nitrogen, resulting in the formation of more chemically stable graphitic nitrogen. Similar changes in the N1s peak ratio were also observed upon doping with other metals, such as Zn, Pt, and Ir.<sup>4,5</sup> Conversely, the pyridinic-to-pyrrolic ratio increased significantly from 8.2 to 19.47, which suggests that the reduction of pyrrolic nitrogen can be attributed to the incorporation of carbon, nitrogen, and oxygen atoms from the DMF molecules that form bonds with melamine in the presence of ZrCl<sub>4</sub>. This interaction transforms the chemical bonding characteristics of the structural surface, which may lead to the formation

of chemical bonds with the surface nitrogen atoms, resulting in a decreased proportion of pyrrolic nitrogen.

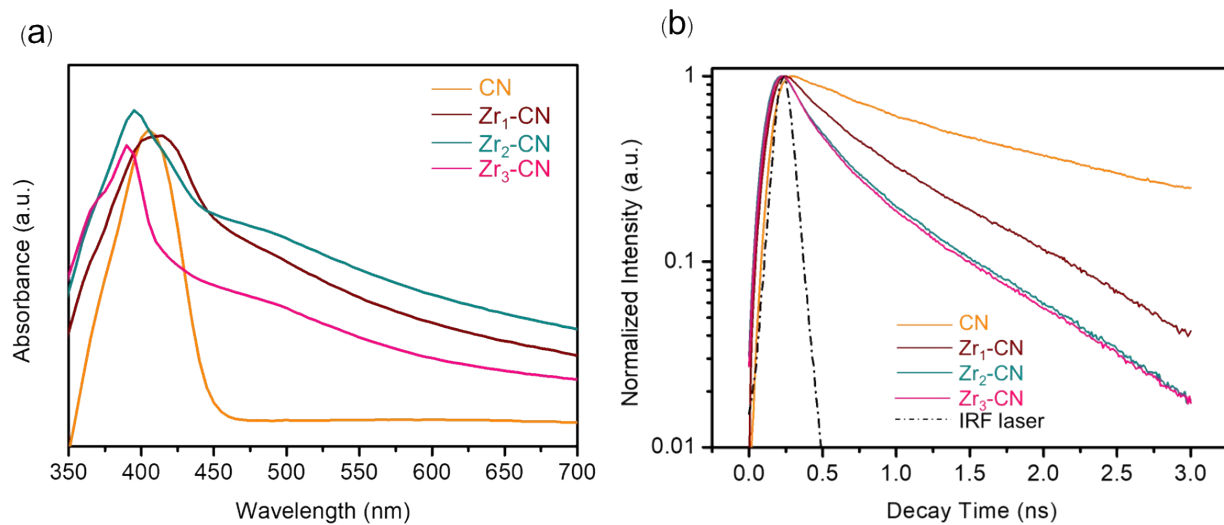


**Figure S7.** (a) Absorbance spectra measured by DRS mode and (b) TRPL spectra lifetime decay of the Zr-doped CN photocatalyst .

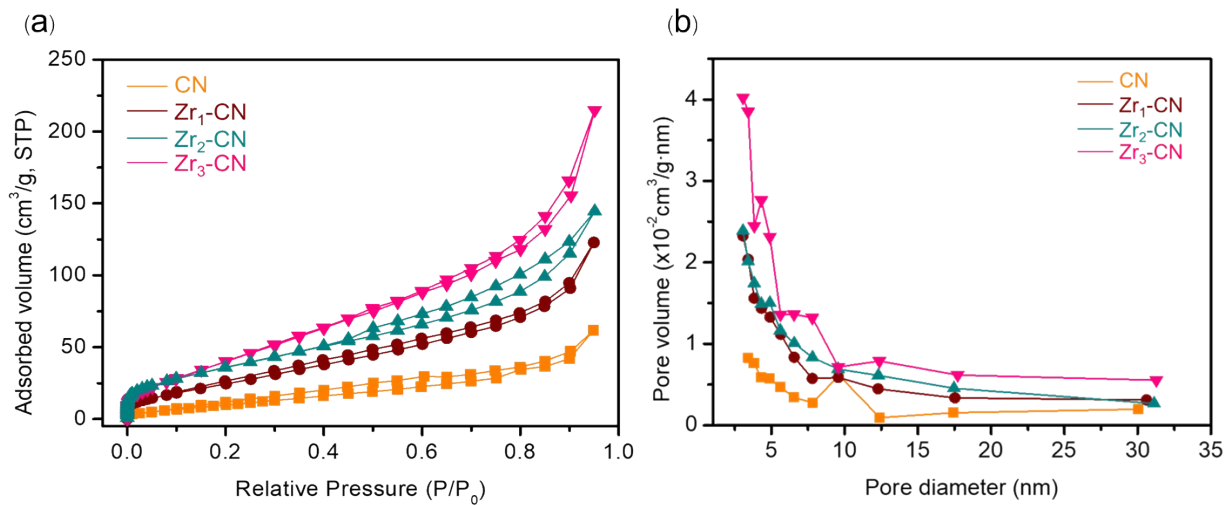


**Figure S8.** (a) BET absorption-desorption isotherm and (b) BJH pore volume and size distribution of the Zr-doped CN photocatalyst.

**Table S4.** Summarization of BET-specific surface area, BJH pore information, and efficiency of photocatalytic degradation of RhB of the Zr-doped CN.

Photocatalyst	BET SSA (m <sup>2</sup> /g)	BJH Pore volume (cm <sup>3</sup> /g) and average pore diameter (nm)	Absorption-desorption	Photocatalytic efficiency (at 540 min)	K value (min <sup>-1</sup> ) and R <sup>2</sup>
No photocatalyst	-	-	0%	1-2 %	-
CN	48	0.095, 3.6	25%	68%	1.6x10 <sup>-3</sup> (0.991)
Zr <sub>1</sub> -CN	98	0.165, 7.7	32%	80%	2.3x10 <sup>-3</sup> (0.992)
Zr <sub>2</sub> -CN	135	0.19, 6.57	33%	98%	7.2x10 <sup>-3</sup> (0.948)
Zr <sub>3</sub> -CN	167	0.3, 7.98	45%	94%	5.1x10 <sup>-3</sup> (0.996)

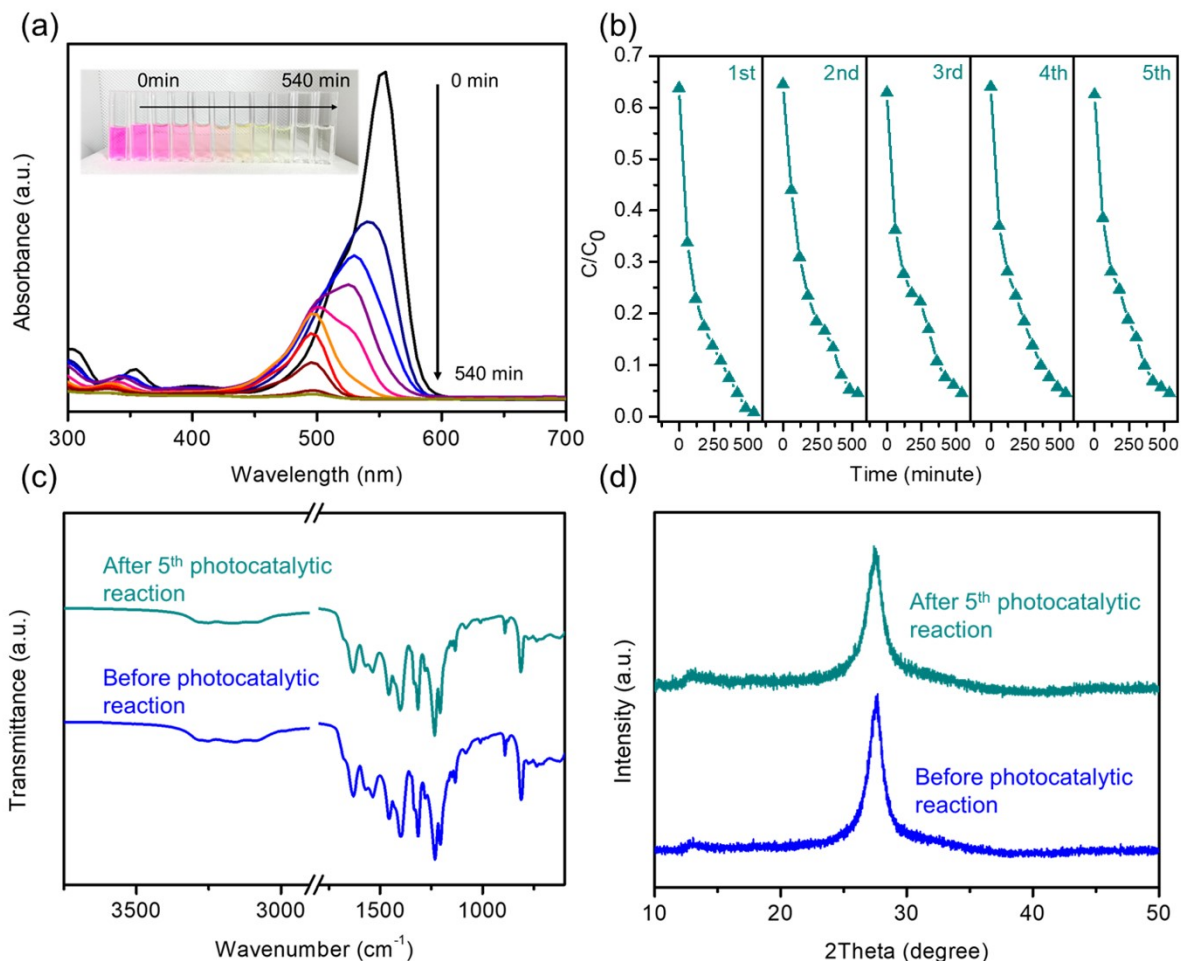


**Figure S9.** (a) Absorbance spectra and (b) cyclic stability of kinetic curve of 10 ppm RhB under photocatalytic degradation using  $Zr_2$ -CN photocatalyst. (c) FTIR spectra and (d) XRD pattern of  $Zr_2$ -CN photocatalyst before and after the 5<sup>th</sup> photocatalytic reaction.

Figure S9(a) shows the absorbance of RhB molecules at various reaction times, and the inset shows the kinetic degradation of RhB at the corresponding times. Figure S9(b) shows the reusability of  $Zr_2$ -CN for the photocatalytic degradation of RhB over five cycles without any change in efficiency. Figure S9(c-d) shows the FTIR spectra and XRD patterns of  $Zr_2$ -CN before and after use for five times cycles of photocatalytic degradation of RhB, indicating that the  $Zr_2$ -CN photocatalyst offers high stability and reusability for practical applications.

## Supplementary references

- 1 X. Peng, J. Li, X. Liu, L. Yi, P. Cai and Z. Wen, *Int J Hydrogen Energy*, 2021, **46**, 28591–28601.
- 2 T. Ji, Y. Guo, H. Liu, B. Chang, X. Wei and B. Yang, *RSC Adv*, 2021, **11**, 31385–31394.
- 3 Y. Wang, X. Tang, P. Huo, Y. Yan, Z. Zhu, J. Dai, Z. Liu, Z. Li and H. Xi, *Journal of Physical Chemistry C*, 2021, **125**, 9646–9656.
- 4 E. Alwin, R. Wojcieszak, K. Kočí, M. Edelmannová, M. Zieliński, A. Suchora, T. Pędziński and M. Pietrowski, *Materials*, DOI:10.3390/ma15030710.
- 5 B. Yue, Q. Li, H. Iwai, T. Kako and J. Ye, *Sci Technol Adv Mater*, DOI:10.1088/1468-6996/12/3/034401.